Some Unsolved Problems in Atmospheric Radiative Transfer: Implication for Climate Research in the Asia–Pacific Region

K. N. Liou, Y. Gu and W. L. Lee

Department of Atmospheric and Oceanic Sciences and Joint Institute for Regional Earth System Science and Engineering, University of California, Los Angeles, California, USA
knliou@atmos.ucla.edu

Y. Chen

Center for Satellite Applications and Research, NESDIS, NOAA, Camp Springs, Maryland, USA

P. Yang

Department of Atmospheric Sciences, Texas A&M University, College Station, Texas, USA

A number of unsolved problems in atmospheric radiative transfer are presented, including the light scattering and absorption by aerosols, the effect of mountains on radiation fields, and radiative transfer in the atmosphere–ocean system, with a specific application to the Asia–Pacific region. We discuss the issues of two nonspherical and inhomogeneous aerosol types, dust and black carbon, regarding climate radiative forcings. Reduction in uncertainties of their radiative forcings must begin with improvement of the knowledge and understanding of the fundamental scattering and absorption properties associated with their composition and size/shape. The effects of intensive topography, such as that in the Tibetan Plateau, on surface radiation and the radiation field above, are significant and the solution requires a three-dimensional radiative transfer program. We show that in a clear atmosphere, surface net solar flux averaged over a mesoscale domain can differ by 5–20 $\mathrm{W/m^2}$ between a slope and a flat surface. Accurate calculations and parametrizations of both solar and thermal infrared radiative transfer in mountains must be developed for effective incorporation in regional and global models. The wind-driven air–sea interface is complex and affects the transfer of solar flux from the atmosphere into the ocean and the heating in the ocean mixed layer. We point out the requirement of reliable and efficient parametrizations of the ocean surface roughness associated with surface winds. The scattering and absorption properties of irregular phytoplankton and other species in the ocean must also be determined on the basis of the rigorous theoretical and experimental approaches for application to remote sensing and climate research.

1. Introduction

Radiative transfer is a subject of study in a variety of fields, including astrophysics, applied physics, optics, planetary sciences, atmospheric sciences, meteorology, and various engineering disciplines. Prior to 1950, radiative transfer was studied principally by astrophysicists, although it was also an important research area in nuclear engineering and applied physics associated with neutron transport. In his groundbreaking book, Chandrasekhar (1950) presented

the subject of radiative transfer in plane-parallel (one-dimensional) atmospheres as a branch of mathematical physics and developed numerous solution methods and techniques. The field of atmospheric radiation, which evolved from the study of radiative transfer, is now concerned with the study, understanding, and quantitative analysis of the interactions of solar and terrestrial radiation with molecules, aerosols, and cloud particles in planetary atmospheres as well as the surface on the basis of the theories of radiative transfer and radiometric observations made from the ground, the air, and space (Liou, 1980, 2002). A fundamental understanding of radiative transfer processes is the key to understanding the atmospheric greenhouse effects and global warming which results from external radiative perturbations of the greenhouse gases and air pollution, and to the development of methods to infer atmospheric and surface parameters through remote sensing. In this article, we present three basic and largely unsolved radiative transfer problems in the climate and weather research with an orientation toward the Asia–Pacific region.

The contemporary scientific issues associated with anthopogenic aerosols in climate change and global warming are profound and their impacts on the environment and human health are of great concern to scientists and the lay public alike. Aerosols are globally distributed in time and space, and affect the Earth's radiation budget by the scattering and absorption of the incoming solar radiation and the emitted thermal infrared radiation in the atmosphere, referred to as the aerosol direct effect, and by modifying the microphysical and radiative properties and lifetime of clouds, referred to as the aerosol indirect effect. The radiative forcings of aerosols both direct and indirect remain the most uncertain elements in the assessment of climate and climate change (IPCC, 2001), owing to our limited knowledge of their chemical and microphysical properties that directly affect the absorption and scattering of radiation, as well as their intricate indirect effects on cloud formation and the consequence of radiation perturbation. We have provided this review of two key aerosol types, dust and black carbon, in terms of their impact on radiative transfer in order to expand our knowledge and understanding of their fundamental scattering and absorption properties in association with satellite remote sensing and application to climate modeling and research.

In addition to aerosols, the transfer of both solar and thermal infrared radiation over mountainous regions complicates the study of radiative transfer. In particular, the temporal and spatial distribution of surface solar radiation over intensive topography results from complex interactions among the incoming direct solar beam, the atmosphere, and the surface. This distribution in turn determines the dynamics of many landscape processes, such as surface heating and moistening, evapotranspiration, photosynthesis, and snow melting. Accurate calculation of radiative transfer is crucial for many fields, including climatology, ecology, and hydrology. Significant progress has been made on land–atmosphere interactions involving vegetation; however, the effect of terrain inhomogeneity on the radiation fields of the surface and the atmosphere above has been largely neglected in weather and climate models. Many landscapes exhibit significant terrain features; for example, the Tibetan Plateau profoundly influences the general circulation of the atmosphere owing to its uplift of large scale flow patterns and its insertion of heating with a confining lower boundary at high levels.

The final issue is one of quantifying the energy transfer across the sea surface, which is essential to understanding the general circulation of the ocean. Solar radiation from the sun contributes most of the heat fluxes that penetrate the air–sea interface and are subsequently absorbed throughout the ocean mixed layer. Thus, solar radiative transfer differs from other air–sea interaction processes, such

as wind stress, evaporation, precipitation, and sensible cooling, which occur only at the sea surface. Radiative transfer in the atmosphere and the ocean requires a specific treatment of the interface between air and water at which the state of the sea surface is largely controlled by surface winds. The scattering and absorption of particulates in the ocean associated with the transfer of solar radiation and the heating in the ocean mixed layer require further research from the perspectives of rigorous electromagnetic scattering theory as well as controlled laboratory experiments.

This paper is organized following the preceding three challenges of radiative transfer and we have made a specific effort to apply these radiation problems as they relate to East Asia. A summary is given in the last section.

2. Light Scattering and Absorption by Aerosols

The importance of the scattering and absorption properties of aerosols for the radiation field and the consequence of their climate impact have been briefly introduced. In this section we first illustrate the climatic radiation effect of aerosols over the East Asia region by employing a general circulation model (GCM) experiment. This is followed by a review of the composition, particle shape, and size of two types of aerosols, dust and black carbon (BC), which are particularly important in climate radiative forcing analysis.

In what follows, we present results of a climate numerical experiment using the UCLA GCM developed by Gu *et al.* (2003, 2006) to illustrate the importance of aerosol optical depth for precipitation simulation in the East Asia region. The yearly and monthly mean aerosol optical depths at the wavelength of $0.75\,\mu$m over China, determined from the data involving the daily direct solar radiation, sunshine duration, surface pressure, and vapor pressure from 1961 to 1990 (Luo *et al.*, 2001), were used to investigate the effects of the observed aerosols in China on climatic temperature and precipitation distributions. The larger aerosol optical depths are found in southern China, with a maximum value of about 0.7. In light of the available satellite data for aerosol-optical-depth climatology and for there to be compatibility and consistency with the long-term surface observations in China, we employed a background aerosol optical depth of 0.2 for the areas outside of China in the GCM simulations to focus our analysis on the effect of localized aerosols on regional climate patterns.

The effect of the aerosol optical depth in China on surface temperature and precipitation patterns was examined by comparing the two GCM experiments — the only difference is that the observed aerosol optical depths in China were used in one experiment and not the other. Since the differences between the two experiments are mainly located in the summer hemisphere associated with the position of the sun, results are presented in terms of the July means for precipitation and outgoing long-wave radiation (OLR) patterns, as shown in Fig. 1. Cooling in the mid-latitudes strengthens the meridional circulation, resulting in increased precipitation in southern China, the Arabian Sea, and the Bay of Bengal, as well as India and Myanmar. To compensate for these increases, a broad band of decreased precipitation is located to the south of the increased precipitation region, with a small decrease to the north. Increase in regional precipitation, especially in the southern part of China and over areas of Indian where abundant moisture is available in summer, appears to be related to the increased aerosol optical depth that occurred in China. Positive differences in OLR are located at higher latitudes, while decreases are found to extend from North Africa to southern China, where precipitation is enhanced, revealing increased convection in this region. In a previous study, Menon *et al.* (2002) suggested that increase in the precipitation in southern China could be related to

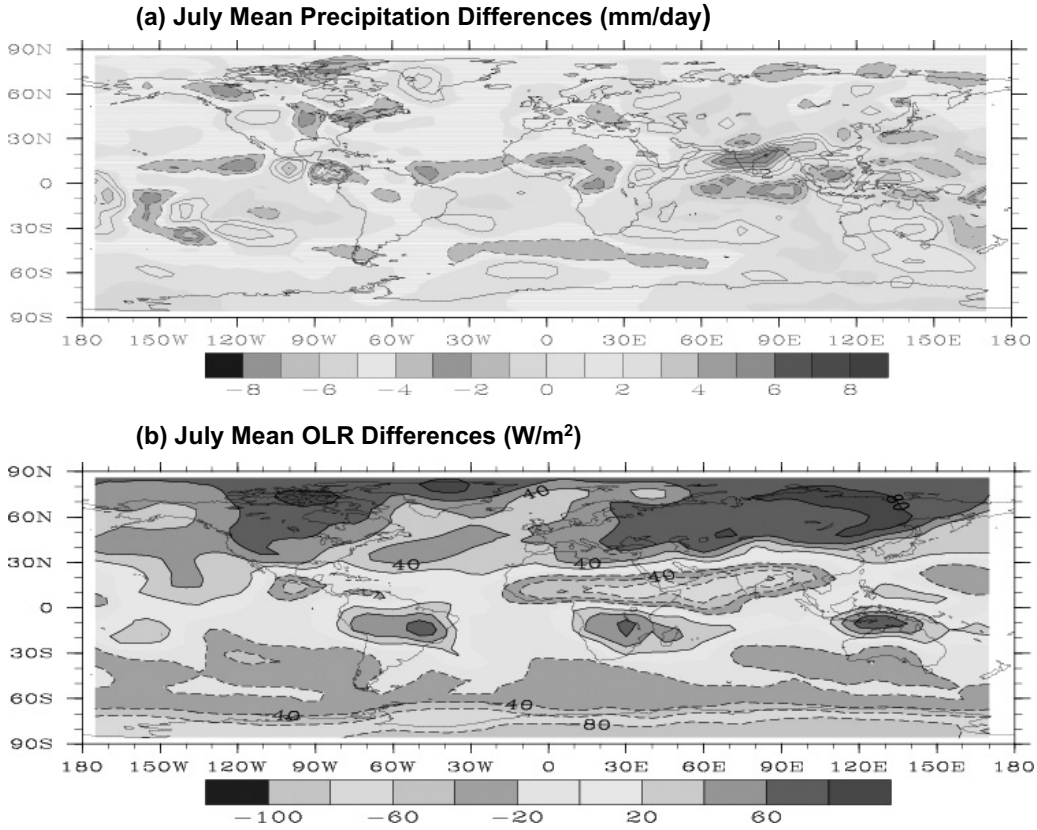

Figure 1. Effect of the aerosol optical depth in China on simulations of the July OLR and precipitation difference patterns determined from the two GCM experiments (denoted as CHIN and AERO in the figure) in which the only difference is that the observed aerosol optical depths in China were used in CHIN (after Gu *et al.*, 2006, with modification).

increase in the absorbing aerosols, a hypothesis which differs from our current finding. This difference illustrates the significance of using the aerosol optical depth (extinction) and single-scattering albedo (absorption) in GCM climate simulations.

Understanding the direct radiative forcing of aerosols requires fundamental knowledge and reliable data on their scattering and absorption properties. The single-scattering properties of aerosols are determined by their dielectric characteristics (refractive index) associated with chemical composition and morphologies in terms of external geometric shape and composition. Aerosol shapes are diverse and span from quasisphere to highly irregular geometry. In addition to complex particle geometry, the inhomogeneous composition of aerosols has been commonly observed. Dust and carbonaceous (particularly BC) particles are two major types of aerosols that profoundly affect climate.

(a) *Dust particles.* Dust can scatter and absorb solar and terrestrial radiation, leading to the positive and negative effects of aerosol direct forcing. Moreover, the solar and infrared radiative forcings of dust may be of different signs, thus further complicating the total forcing assessment. Determination of the sign and magnitude of direct radiative forcing by dust on regional and global scales remains a key unsolved problem (e.g. Sokolik *et al.*, 2001).

With respect to the chemistry and composition of dust particles, Falkovich *et al.* (2001) conducted chemical and mineralogical analysis of dust particles collected in a dust storm over Israel and found that dust particles typically occur in aggregated form with varying mineralogical composition, consisting mostly of Ca, Mg, Al, and Si. Analysis also showed that sulfur (S) and iron (Fe) adhered to the particle's surface, which was suggested to have occurred from processes within the source region. Gao *et al.* (2001) studied the characteristics of soil-based aerosols originating in China and the effects of global transport on the composition and reported that the mineralogy of the loess soil primarily consists of quartz (SiO_2), feldspars, micas, clays as well as carbonates ($CaCO_3$ in particular) and other trace minerals. Mineralogy of dust particles is a function of geographical location. Near the source region, dust assumes the composition of its parent soil; however, when dust is transported over large distances, the composition will change depending on the direction of the dust plume. For example, airborne dust passing through an urbanized region may mix with local pollutants such as black carbon or it may mix with sodium chloride crystals as it gets transported over the oceans inside the marine boundary layer. Mineral dust rarely exists as a pure mineral, but rather, owing to internal and external mixing, as a complex aggregate of several minerals. Sokolik *et al.* (1998) extensively studied the optical properties of a wide range of dust mixtures. Major minerals investigated thus far include quartz, common clays, (montmorillinite, illite, and kaolinite, to name a few), and the carbonates dolomite and hematite, the latter is responsible for the redness sometimes seen in visible observations. Large uncertainties exist as to how to best represent these minerals in an optical model for radiative flux calculations and remote sensing applications.

Characterizing the shape of a dust particle is a difficult and challenging process. Through laboratory analysis and *in situ* measurements using the scanning electron microscope, 2D particle shape can be inferred by using one of several shape parameters. One commonly used parameter is circularity, which is defined as $C = L^2/4\pi A$, where L is the particle's perimeter (μm) and A is the 2D projection area of the particle (μm^2). $C = 1$ refers to a circular particle, and a square has a C equal to 1.27. Dust partcles typically have C values ranging from 1 to as high as 4 or 5. Based on histograms from the dust samples collected in China, the bulk of C values range from 1 to 2 (Gao *et al.*, 2001). Recent individual analysis data on Saharan dust particles show that as particle size increases, as is the case during heavy dust outbreaks, so too does its circularity, indicating that dust is rarely spherical. Most dust particles are highly irregular and angular, possessing sharp corners (Koren *et al.*, 2001; Gao *et al.*, 2001). They also tend to be elongated in a direction perpendicular to their rotational axis; that is, they are oblate. Typical aspect ratios for dust particles observed during studies in China (Okada *et al.*, 2001) and the PRIDE field experiment (Reid *et al.*, 2003) are in the range of 1.4–1.9. Previous studies have made many assumptions regarding the shape of dust particles. Dust is commonly composed of quartz crystals that are typically tetrahedral in shape. Particles composed of clays have been observed to exhibit flat, platelike structures. The scattered intensity of irregular aerosols could be a factor of 1.5 larger and a factor of 2 smaller at forward scattering and backscattering angles, respectively, than those of volume-equivalent spheres (Kalashnikova and Sokolik, 2002).

Many studies have been dedicated to quantifying the size distribution of dust particles from varied global locations over the years, but data interpretation and problems with sizing techniques have large uncertainties (Reid *et al.*, 2003). d'Almeida *et al.* (1991) characterized the size spectrum assuming a lognormal distribution, which can often be bimodal. Some

typical size distributions cited in contemporary works on dust research also suggested a gamma distribution with an effective radius of about $2\,\mu$m.

Satellite remote sensing of the optical depth and size of dust particles can be used to constrain GCM simulations concerning the impact of dust outbreaks on climate and climate change. As discussed above, dust particles are exclusively nonspherical. However, it has been a common practice to use the phase function computed from the Lorenz–Mie theory for "equivalence" spheres in retrieval and analysis. On the basis of the scattering results for spheroids, Mishchenko *et al.* (1995) illustrated that the spherical equivalence assumption can result in substantial errors in the aerosol optical depth retrieved from satellite observations. Dubovik *et al.* (2006) further showed that this assumption can lead to unrealistic retrievals in aerosol size distribution and the spectral dependence of the refractive index inferred from ground-based AERONET measurements. It appears that the significance of aerosol nonsphericity in remote sensing and climate study has been increasingly recognized.

In the following, we present an example of the importance of aerosol nonsphericity for satellite remote sensing and radiative forcing analysis. Figure 2 displays the phase functions at a wavelength of $0.63\,\mu$m and with a size parameter of 10 for three types of aerosol particles — a randomly oriented dustlike particle with 10 surface faces, a spheroid, and a sphere — computed with the finite-difference time domain (FDTD) approach (Yang and Liou, 2000), the T-matrix method (Mishchenko *et al.*, 1996), and the Lorenz–Mie theory, respectively. The two top panels are for oceanic particles at the two satellite sensing wavelengths of 0.63 and $0.86\,\mu$m, while the bottom panels are for mineral and soot particles using a wavelength of $0.63\,\mu$m. As shown, significant differences are evident in the backscattering directions where satellite radiometers see the atmosphere, except in the case of soot with large absorption, denoted by a significant value in the imaginary refractive index. These differences can be as large as a factor of 10 between dustlike and sphere at most of the scattering angles greater than 120°. If the retrieval uncertainty for optical depth, τ, is 50%, defined as $[\tau(\text{dust}) - \tau(\text{sphere})]/\tau(\text{sphere})$, the aerosol solar radiative forcings at the top of the atmosphere (TOA) and the surface differ by 8 and $12\,\text{W/m}^2$, respectively, based on calculations from the Fu and Liou (1992, 1993) radiative transfer model using the standard atmospheric profiles for water vapor and other gases along with a solar constant of $1366\,\text{W/m}^2$, a surface albedo of 0.1, and a solar zenith angle of 60°. A retrieval uncertainty factor of 2 yields radiative forcing differences of 15 and $23\,\text{W/m}^2$ at TOA and the surface, respectively. These are hypothetical large numbers for illustration purposes but nevertheless a physically reliable remote sensing of aerosol optical depth must account for the aerosol nonsphericity, particularly in the case of dust.

(b) *Carbonaceous particles.* Carbonaceous particles in the atmosphere, which are of specific interest to the climate and climate change study, strongly absorb sunlight, heat the air, and contribute to global warming (Menon *et al.*, 2002). Recent investigations indicated that the magnitude of the direct radiative forcing due to BC exceeds that from CH_4 and may be the second most important component of global warming, after CO_2, in terms of direct forcing (Jacobson, 2001). In addition to the direct climate effect, BC particles, acting as CCN, can inhibit cloud formation (Koren *et al.*, 2004). The magnitude of BC absorption depends highly on its refractive index (especially its imaginary part), shape, and size distribution. It also depends on the mixing state of BC particles.

Carbonaceous compounds make up a large but highly variable fraction of the atmospheric aerosols. Carbonaceous materials are byproducts of solid, liquid, or vapor combustion,

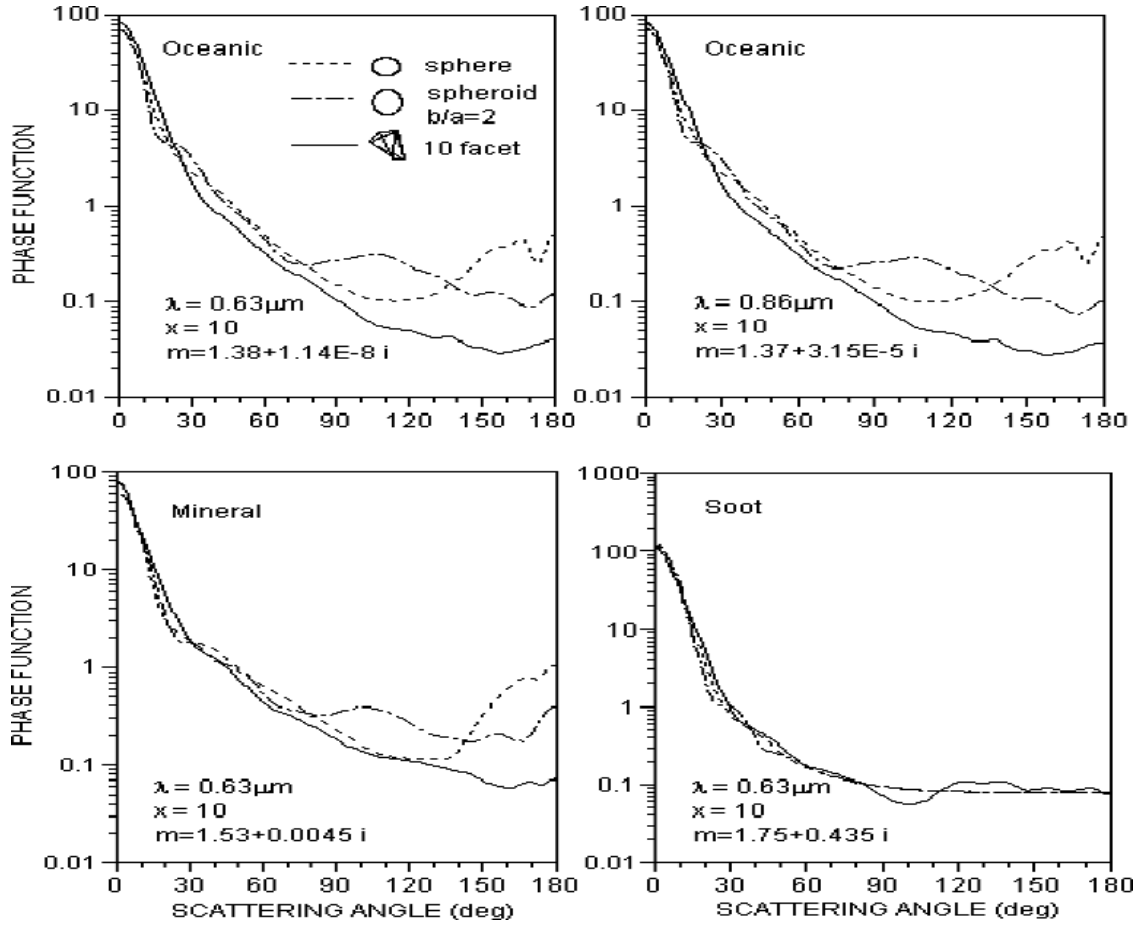

Figure 2. Phase functions at a wavelength of 0.63 μm and with a size parameter of 10 for three types of aerosol particles: a randomly oriented dustlike particle with 10 surface faces, a spheroid, and a sphere computed with the finite-difference time domain (FDTD) approach, the T-matrix method, and the Lorenz–Mie theory, respectively.

generated either directly through aggregation of molecules formed in combustion processes from coal, biomass burning, and biofuel, leading to soot particles (primary carbon), or indirectly through condensation from a supersaturated gas produced by chemical reactions and resulting in secondary organics (secondary carbon). The by-products of fossil fuel burning are injected into the atmosphere from both stationary sources, such as factories and power plants, and mobile sources, such as motor vehicles. Aerosol particles produced by fossil fuel burning are concentrated over North America, Europe, China, Japan, India, and other industrialized regions. The primary aerosol particles released from fossil fuel burning generally fall into two categories: soot and fly ash. Soot includes both elemental (BC) and organic compounds, and is generally in the fine particle mode. Fly ash is the nonorganic by-product of coal burning. Coal contains substantial residual mineral material, including clays, shale, sulfides, carbonates, chlorides, and various trace metals. When coal is burned, these parent materials are released unreacted or thermally transformed. They take the form of spherical glassy particles in the coarse particle mode. The combination of soot and fly ash released from coal furnaces results in a bimodal size

distribution of primary aerosol particles. Diesel engines are the dominant source of soot in some urban environments, but worldwide, coal burning releases about ten times as much BC into the atmosphere as diesel fuel combustion.

Primary carbon or soot aerosol consists of two subcomponents with different absorbing features: graphitic carbon with a high absorbing property and primary organics with a rather weak absorbing property (Rosen and Novakov, 1984). The number and mass concentrations of the single subcomponents are highly variable functions of space and time, as in the case of the parameters determining their size distribution. Given this importance, measurements of BC and the differentiation between BC and organic carbon still require improvement (IPCC, 2001). Recent estimates place the global emission of BC aerosols from biomass burning at 6–9 Tg/yr and from fossil fuel burning at 6–8 Tg/yr (Scholes and Andreae, 2000). The emission of BC has been especially large in China, owing to the low temperature household burning of coal and biofuels (Streets *et al.*, 2001). Giorgi *et al.* (2002) carried out a series of simulations using a coupled regional climate-chemistry/aerosol model and showed that anthropogenic fossil fuel soot exerts a positive radiative forcing of 0.5–2 W/m^2 TOA. Using a regional climate model developed in China, Wu *et al.* (2004) also reported that BC induces a positive radiative forcing at TOA and a negative forcing at the surface. Reducing uncertainties in the radiative forcing due to BC must account for its fundamental absorption and scattering properties.

BC particles can be internally and externally mixed with other nonabsorbing materials (Martins *et al.*, 1998). The same amount of BC under different types of mixing can result in fairly different absorption properties. The efficiency of absorption of a certain amount of BC is determined by its mass absorption coefficient, which depends on the size of particles and the type of mixing between BC and nonabsorbing components such as organic matter and sulfates. In the case of an external mixture where individual pure BC particles are in parallel with nonabsorbing particles, the BC mass absorption efficiency is about the same for pure BC particles. However, it is likely that BC particles that form at relatively high temperature will be coated by a nonabsorbing shell to form an internal mixture. Another type of internal mixture is a long-chain aggregate of BC particles formed at high temperature, which can also be coated with nonabsorbing materials to form an internally mixed heterogeneous structure. These opened clusters usually collapse to form closely packed sphertlike structures as a result of interactions with water vapor and clouds.

Owing to their production mechanisms, carbonaceous materials, including BC, are confined to the submicrometer size range. However, aggregation of freshly produced particles may yield particle sizes above that range. Small spherical soot particles coagulate to form chainlike aggregates. These irregularly shaped particles have been found to be fractal, and have special optical properties. The mass median diameter of BC in the atmosphere is very small, between 0.1 and 0.5 μm. In urban air, two size modes can often be detected; a smaller mode resulting from freshly formed primary aerosol and a larger mode resulting from coagulation processes. The more remote the location, the more dominant the larger size mode, reflecting the importance of coagulation during the aging of carbonaceous aerosol as it is transported from the site of combustion. BC aerosols normally have a long lifetime in the atmosphere because of their small size, usually less than 1 μm. Identifying and quantifying the purely carbonaceous material remains a difficult task. Effects of the aggregation of soot aerosols on their scattering and absorbing properties have recently been studied by Liu and Mishchenko (2005).

The state-of-the-art radiative transfer schemes that have been used in climate models have not taken into account the effects of aerosol nonsphericity and inhomogeneous structure

(e.g. Gu *et al.*, 2006, and the preceding GCM example). The neglect of these effects could substantially underestimate or overestimate aerosol radiative forcing. For example, the asymmetry factor of realistic aerosols, which is directly related to the albedo effect, can be quite different from that of their spherical counterparts. It follows that a spherical "equivalence" assumption can lead to erroneous assessment of the aerosol radiative forcing. In the preceding discussion, we have demonstrated the nonspherical shape effect of dust particles on the scattering phase function and the consequence of remote sensing of their optical depth and particle size. In the case of BC particles, we have showed the complexity of inhomogeneity associated with internal inclusions, external attachments, and cluster structures. Indeed, accurate and efficient determination of the scattering and absorption properties of these two major types of nonspherical and inhomogeneous aerosols is a subject that will require in-depth research efforts.

3. The Effect of Mountains on Radiation Fields

The energy emitted by the Sun and received by the Earth's surface is determined by three sets of factors. The first includes the latitude, the solar hour angle, and the Earth's position relative to the Sun, which determine incoming solar radiation at the top of the atmosphere and can be precisely calculated (Liou, 2002). The second involves the attenuation of the solar beam by scattering and absorption caused by atmospheric gases, aerosols, and cloud particles. The last comprises terrain characteristics including elevation, slope, orientation, and surface albedo. On a sloping surface in mountainous terrain, the total solar radiation can be separated into five components according to the Sun-to-surface path (Fig. 3): (1) the direct flux contains the photons arriving on the ground directly in line from the Sun to the surface, unscattered by the atmosphere; (2) the diffuse flux is composed of photons scattered by the atmosphere; (3) the direct-reflected flux is associated with photons traveling directly through the atmosphere unscattered but subsequently reflected to the target surface by neighboring slopes; (4) the diffuse-reflected flux is similar to the direct-reflected irradiance except that it is composed of photons already scattered by the atmosphere and then reflected by neighboring slopes; and (5) the coupling flux is composed of photons that have experienced multiple surface reflections and atmospheric scatterings. The direct, diffuse, and coupling components are produced when solar radiation interacts with a flat surface. However, over mountains, additional components are generated by the direct-reflected and diffuse-reflected fluxes through interaction with rough topography that are absent for the flat surface.

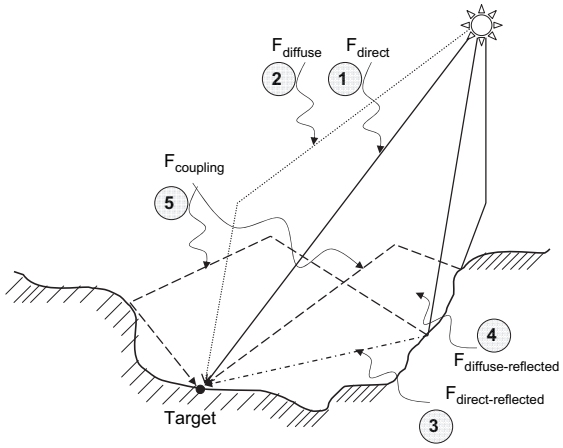

Figure 3. Schematic representation of the flux components received by the target on a sloping surface in mountainous terrain. (1) direct, (2) diffuse, (3) direct-reflected, (4) diffuse-reflected, and (5) coupling fluxes (after Chen *et al.*, 2006).

A variety of models of varying sophistication and complexity have been developed to compute most of these solar flux components in rugged terrain in which the direct incident beam is computed by introducing a cosine correction of the local zenith angle and considering the shadow caused by topography

(e.g. Olyphant, 1986). Diffuse radiation has been modeled as being proportional to the area of the sky dome visible to the target surface (e.g. Dozier and Frew, 1990). Factors contributing to terrain-reflected flux have generally not been considered explicitly, but are approximated by assuming a first-order reflection between surrounding terrain and the target surface. The terrain-reflected radiation is particularly significant over snow surfaces (Dozier, 1980). Miesch *et al.* (1999) used a Monte Carlo approach to compute flux components at ground level and the radiance reaching the satellite-borne sensor over a very simple 2D rugged terrain with homogeneous atmospheric layers above, and concluded that a 10% error may occur when the terrain-reflected and coupling components may play a dominant role in the signal measured by a satellite sensor over poorly exposed or shadowed areas. As this brief literature survey illustrates, the effect of complex 3D mountainous terrain on the surface flux components of Fig. 3 has not been systematically and rigorously studied.

Chen *et al.* (2006) developed a 3D Monte Carlo radiative transfer model that calculates the flux components exactly given a realistic distribution of scatterers and absorbers in the atmosphere and provided the first definitive assessment of the relative importance of the flux components in a clear-sky atmosphere. The 3D Monte Carlo method for the transfer of radiation from the Sun as a point source with application to clouds has been presented in some detail by Marshak and Davis (2005). Chen *et al.* (2006) also characterized the factors controlling diurnal, seasonal, and geographical variability in the flux components and determined the significance and sources of errors in conventional radiative transfer schemes in areas of intense topography by applying the 3D radiative transfer model to a real 3D mid-latitude mountainous surface. Errors in radiative transfer schemes that have been used in GCM's with smoothed topography were assessed by comparing 3D results with the mountainous surface to identical calculations for a flat surface with the same mean elevation. It was shown that the errors are on the order of 5–20 $\mathrm{W/m^2}$, depending on the time of the day, and stem from the fact that the atmosphere absorbs a different amount of solar radiation when the topography underneath it is smoothed.

The Tibetan Plateau, which covers about 2.4 million square kilometers with an average height of over 4 km, has a profound influence on the general circulation of the atmosphere, owing to its uplift of large scale flow patterns and its insertion of heating with a confining lower boundary at high levels. The wintertime dynamic effect enhances the southward transport of the Siberian high and leads to a large trough in the jet stream extending into the Pacific (e.g. Charney and Eliassen, 1949). The summertime elevated heat source has been recognized by meteorologists since early papers by T. C. Yeh (Ye, 1979) in conjunction with the formation and maintenance of the Asian summer monsoon, the onset of Meiyu, or the East Asian summer monsoon rainfall period, and the summertime heavy rainfall frequently occurring in central China. At lower levels the mechanism is similar to but more powerful than that of the summer near surface jet of the US' Great Plains. However, our knowledge of the Tibetan Plateau heating and its interactions with the complex regional dynamics and the consequent effects has remained rather limited. Although reanalysis data have been used to provide temporal and spatial distributions of differential heating, these results are severely limited by inadequacies in the formulations of diabatic processes in the models. Problems associated with the vertical profile of radiative heating rates over the mountainous region, the coupling of the surface to the lower atmosphere through boundary layer convection, and the snow albedo feedback in regional and global climate change appear to be largely unresolved and often ignored.

We applied the 3D solar radiative transfer model constructed by Chen *et al.* (2006) to a domain of 200 km × 200 km centered at Lhasa over the Tibetan Plateau and carried out an analysis of the topography effects on the surface and atmospheric radiation fields. For the terrain information, we used the HYDRO1k database that was developed at the US Geological Survey's EROS Data Center to provide comprehensive and consistent global coverage of topographical datasets. The required data for radiation calculations include digital terrain elevation, slope, and orientation. Employing the ISCCP 2.5° by 2.5° resolution surface albedo map, we obtain one surface albedo value for radiation calculations. Figure 4 displays the distributions of the surface downward (upper panels) and net (lower panels) solar fluxes at a 1 km × 1 km resolution over the domain. The standard atmospheric water vapor and other trace gaseous profiles were used as input in the calcuation along with a solar zenith angle of 64° and two azimuthal angles correponding to early morning and late afternoon. The results displayed in these diagrams illustrate the effect of terrain and its orientation with respect to the Sun's position. We see substantial different flux values along the river valleys (two heavy solid lines). The net surface solar flux for a flat surface at an average height of abour 4 km is 400 W/m^2, but it varies from about 40 to 500 W/m^2 in the 200 km × 200 km domain. Figure 5 illustrates a 3D atmospheric heating rate distribution in the domain, with the

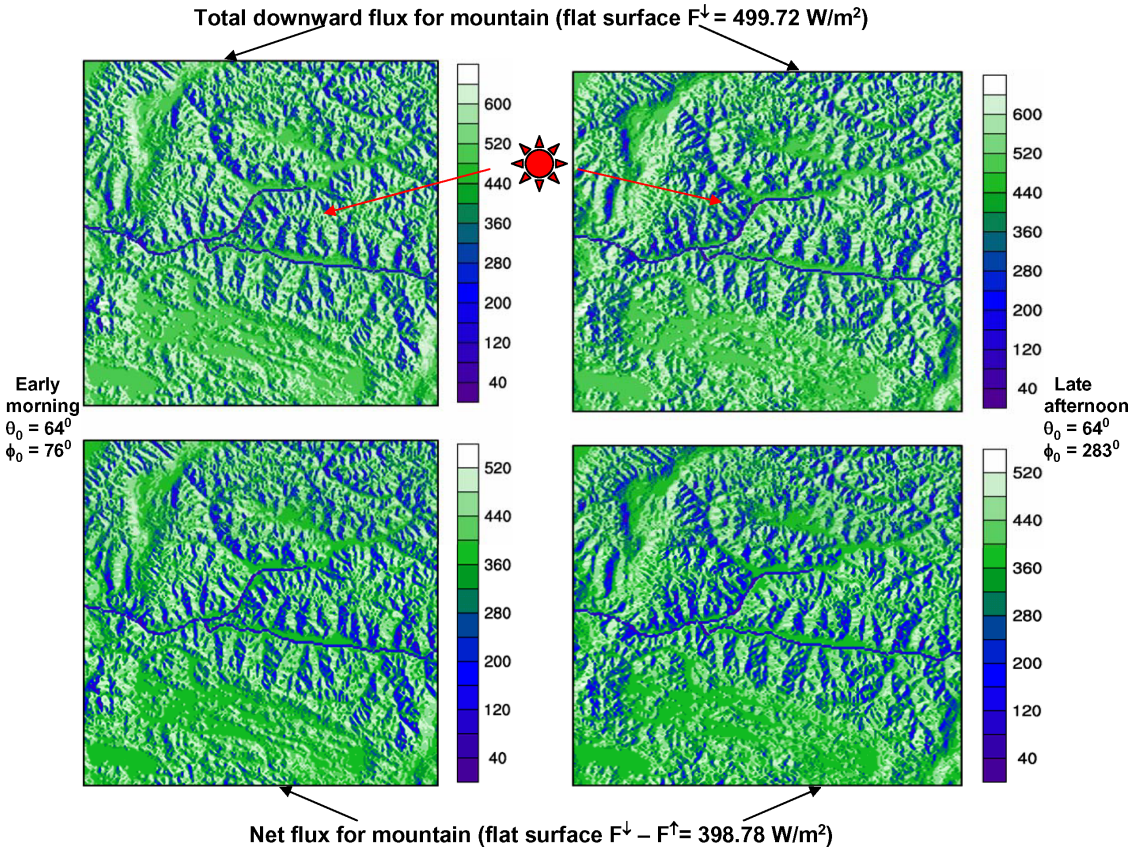

Figure 4. Distributions of the surface downward (upper panels) and net (lower panels) solar fluxes at a 1 km × 1 km resolution over the domain.

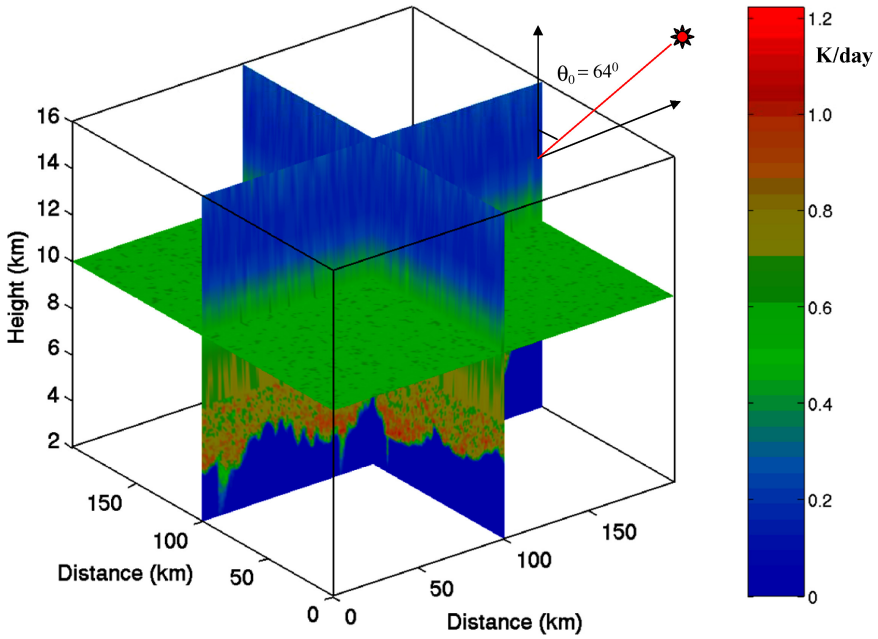

Figure 5. 3D atmospheric heating rate distribution in a 200 km × 200 km domain, with the terrain height shown at the bottom as a black shade.

terrain height shown at the bottom as a black shade. A substantial variability of the atmospheric heating rate ranging from about 0.2 to 1.2 K/day is shown. The inhomogeneous surface feature affects not only surface radiation but also the atmospheric radiation field above.

For application to regional weather and climate models, we are most interested in the flux averaged over a domain. Figure 6 illustrates the domain-averaged fluxes for flat and mountain surfaces as a function of time of day using horizontal resolutions of $50\times50\,\mathrm{km}^2$, $100\times100\,\mathrm{km}^2$, and $200\times200\,\mathrm{km}^2$. Two surface albedos of 0.2 and 0.7, representing a snow condition, were used in the calculations. The domain-averaged fluxes were obtained by averaging the results from the $1\times1\,\mathrm{km}^2$ 3D radiative transfer calculations. Net flux differences between the preceding resolutions appear to be small but, in comparison with the flat surface counterpart, a difference of 5–20 $\mathrm{W/m}^2$ is shown. Figure 7 illustrates the averaged atmospheric solar heating rate over a horizatal domain of 200 km × 200 km for the case of a flat surface with an average height of 4.7 km and two mountainous cases representing morning and afternoon conditions. Heating rate results for the two mountaineous cases are close because of the large domain average. However, significant variations from about 0 to about 0.76 K/day are shown in the regions from the lowest elevation of 2.3 km to about 6 km, resulting from the effect of mountain slopes associated with the solar zenith angles used in the calculations. These differences would have a substantial effect on the energy balance of the planetary boundary layer in GCM simulations over the Tibetan Plateau.

In summary, we have demonstrated the significance of topographical effects on surface and atmospheric radiation fields in clear atmospheres. Clouds and aerosols are anticipated to have a profound influence on the radiation budget over mountain terrain and are subject further investigation. Moreover, the thermal infrared (long wave) radiation emitted from rugged terrain with nonhomogeneous surface

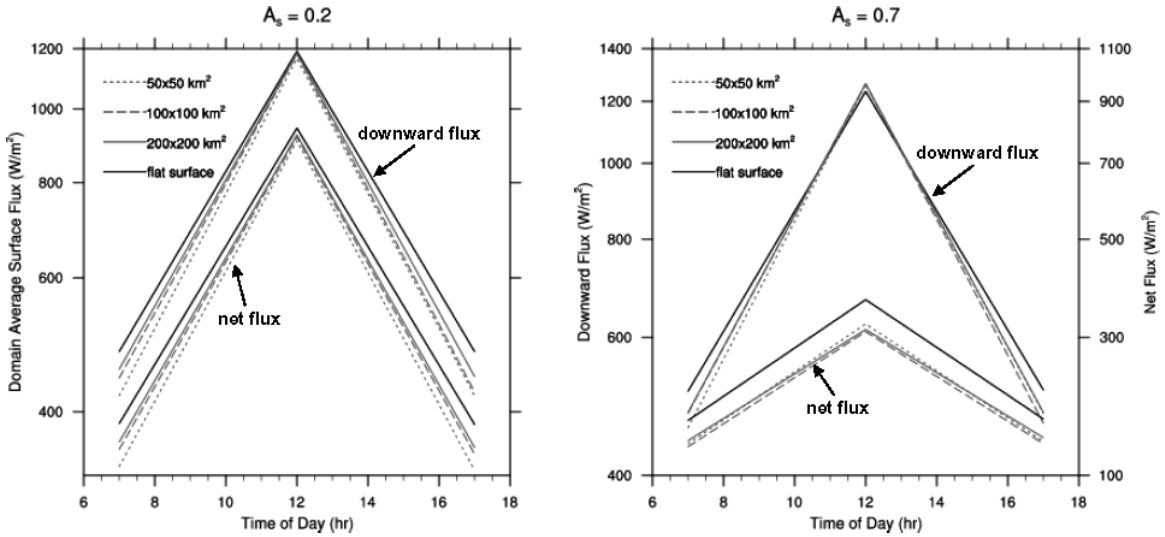

Figure 6. Domain-averaged fluxes for flat and mountain surfaces as a function of time of day using horizontal resolutions of $50 \times 50\,\mathrm{km}^2$, $100 \times 100\,\mathrm{km}^2$, and $200 \times 200\,\mathrm{km}^2$. Two surface albedos of 0.2 and 0.7 (snow condition) were used in the calculations.

temperatures is another subject that requires in-depth study.

4. Radiative Transfer in the Atmosphere–Ocean System

The climatological value of solar flux penetrating the mixed layer can reach $40\,\mathrm{W/m}^2$ in the tropical regions and produce a difference in the heating rate of a 20 m mixed layer by about 0.33°C a month (Ohlmann *et al.*, 1996). The vertical distribution of solar flux also influences the stability and stratification of the mixed layer and the sea surface temperature. Consequently, a quantitative understanding of the ocean solar flux profile is important to ocean model simulations. The surface albedo, which includes the surface reflectivity and the upwelling radiation from the water surface, is critical to the energy budget in the atmospheric planetary boundary layer. However, the reflectivity of the wind-blown surface is difficult to evaluate. The surface reflectance may be reduced by 50% when the solar zenith angle is 70° and the wind speed increases from 0 to 20 m/s (Mobley, 1994).

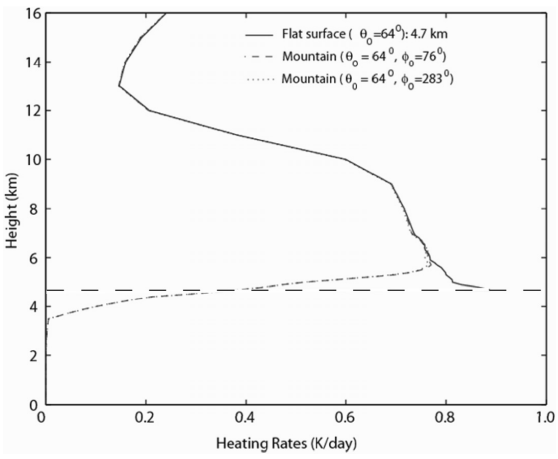

Figure 7. Averaged atmospheric solar heating rate over a horizatal domain of 200 km × 200 km for the case of a flat surface with an average height of 4.7 km (denoted by the horizontal dashed line) and two mountainous cases representing morning and afternoon conditions.

The surface roughness also affects the upwelling radiation from the water surface and its determination requires accurate radiative transfer analysis. In addition, the oceanic pigment on radiative transfer in the ocean is also significant. A change of $0.10\,\mathrm{mg/m}^3$ in the phytoplankton

concentration in the mixed layer can result in a corresponding change of the penetrative solar flux by about $10\,\mathrm{W/m^2}$ at a level of 20 m depth (Siege *et al.*, 1995). Because solar radiation is the energy source for photosynthesis, it also directly affects the marine productivity.

A typical coupled radiation model deals with parametrized and simplified radiative transfer in the atmosphere and ocean separately by considering one medium as the boundary condition or the other. Computationally expensive models have also been developed for solar flux calculation (Jin *et al.*, 2002), but they are not compatible with coupled atmosphere–ocean models for climate simulation.

Lee and Liou (2007) developed a coupled atmosphere–ocean broadband solar radiative transfer model based on the analytic delta-four-stream approach originally derived by Liou (1974) and Liou *et al.* (1988). This approach is computationally efficient and at the same time can achieve acceptable accuracy for flux and heating rate calculations in the atmosphere and the oceans. Figure 8 illustrates a coupled atmosphere–ocean system with the solar beam reflected and refracted by a wind-blown sea surface. For an optically inhomogeneous system, the atmosphere and the ocean can be divided into a number of separate homogeneous layers such that each layer can be characterized by a single-scattering albedo, a scattering phase function, and an extinction coefficient. The entire radiative transfer system can be solved by matching the continuity equations for discrete intensities at the interfaces. To take into account the reflection and transmission of the wind-blown air–water interface, a Monte Carlo method (e.g. Preisendorfer and Mobley, 1985) has been employed to simulate the traveling of photons and to compute the reflectance and transmittance of direct and diffuse solar fluxes at the ocean surface using Cox-Munk's (1954) surface slope distribution. For the ocean part, existing bio-optical models, which correlate the concentration of chlorophyll and the absorption and scattering coefficients of phytoplankton and other matter, have been integrated into this coupled model.

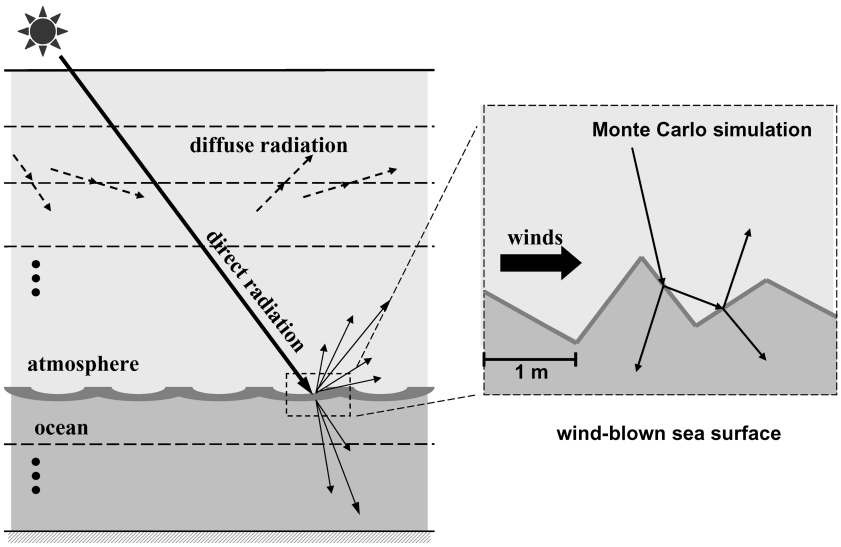

Figure 8. A coupled atmosphere–ocean system with the solar beam reflected and refracted by a wind-blown sea surface. For an optically inhomogeneous system, the atmosphere and the ocean can be divided into a number of separate homogeneous layers such that each layer can be characterized by a single-scattering albedo, a scattering phase function, and an extinction coefficient.

Lee and Liou's model was first compared to the values computed by a more exact model employing more discrete streams and illustrates that the relative accuracies of the surface albedo and total transmission in the ocean determined from the present model are generally within 5%, except in cases of the solar zenith angle being larger than 80°. The observational data collected at the CERES Ocean Validation Experiment (COVE, Jin *et al.*, 2002) site have also been used to validate this model and the results show that the relative differences of downward and upward short wave fluxes and albedo are within 10% of the observed values.

As an example, Fig. 9(a) shows the surface solar albedo as a function of the wind speed and the cosine of the solar zenith angle (SZA), μ_0, for the clear sky condition with the chlorophyll concentrations of 0 and 12 mg/m^3. An ocean depth of 200 m with an ocean bottom albedo of 0.1 was used in the calculation and the chlorophyll concentration was considered uniformly in the whole layer. The sea surface albedo generally increases with the SZA for $\mu_0 > 0.1$, because the Fresnel reflectance increases with an increasing incident angle. However, the surface albedo decreases with the SZA for $\mu_0 < 0.1$, because when the Sun's altitude becomes lower, the intensity of direct solar radiation decreases more rapidly than that of diffuse radiation. Thus, the addition of the proportion of diffuse radiation reduces the effective SZA, leading to decrease in the surface albedo. The wind effect on the surface albedo is strong only when $\mu_0 > 0.4$. The surface albedo increases with chlorophyll concentration owing to increase in the scattering coefficient. However, this effect is not significant because increase in backscattering is canceled out by increase in the particulate absorption in sea water. Figure 9(b) shows the transmission ($z = 5$ m) using the chlorophyll concentrations of 0 and 2 mg/m^3. Transmission decreases significantly with increasing chlorophyll concentration owing to increase in absorption. The transmission minimum occurs at $\mu_0 \sim 0.25$. Owing to Rayleigh scattering, the intensity in the blue light region of direct solar radiation decreases with increase in optical depth. Sea water has a minimum absorption coefficient in the blue light region and for this reason the transmission decreases with an increasing SZA. Because there is more radiant intensity in the blue light region for diffuse radiation than the direct counterpart, the transmission increases with the SZA for the low Sun's elevation associated with more energy for diffuse radiation.

The existing bio-optical models, which correlate the concentration of chlorophyll and the absorption and scattering coefficients of phytoplankton and other matter, are highly empirical and require verification by fundamental theory and observations. For example, absorption by phytoplankton and the associated living or nonliving derivatives and absorption by the dissolved yellow matter are directly correlated with that by phytoplankton without rigorous physical fundamentals. Moreover, the Rayleigh scattering theory is not applicable to water because the distance between water molecules in the liquid phase is too short. The Einstein–Smoluchowski theory (Mobley, 1994) of scattering states that fluctuation in the molecular number density due to random molecular motions causes fluctuation in the index of refraction, which gives rise to scattering. An empirical form for the volume scattering function and the scattering coefficients between 200 and 800 nm for pure sea water have been used in the field of ocean optics (Smith and Baker, 1981). In addition, the scattering coefficients for phytoplankton and other matter have been determined simply from the bio-optical model (Morel and Maritorena, 2001). The correct scattering and absorption properties for irregular phytoplankton and other species in the ocean must be determined from the theory of electromagnatic scattering along with appropriate scattering experiments in the laboratory — an exciting research area.

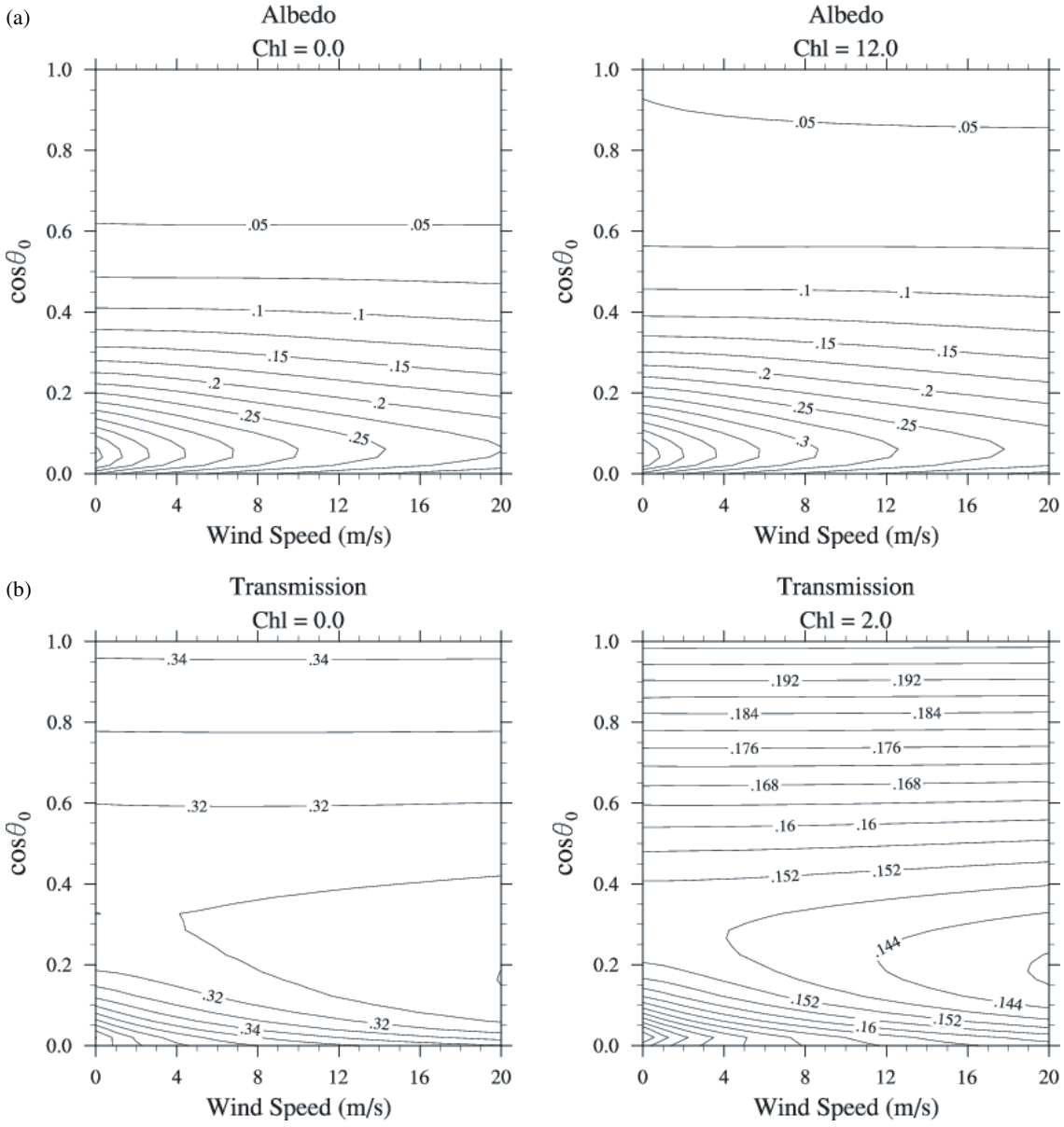

Figure 9. (a) Sea surface albedo for radiation between 0.2 and 4.0 μm as a function of the wind speed and the cosine of the solar zenith angle for the clear sky condition with chlorophyll concentrations of 0 (left panel) and 12 (right panel) mg/m^3. (b) Transmission at the ocean depth of 5 m with chlorophyll concentrations of 0 (left panel) and 2 mg/m^3 (right panel) (after Lee and Liou, 2007).

5. Summary

In this paper, we have presented three contemporary and largely unsolved problems in atmospheric radiative transfer with application to the Asian–Pacific region. Although it has been written in a review format, some new results have also been presented to illustrate important points in climate and remote sensing applications.

Aerosols are undoubtedly the most uncertain climate element in the Earth's atmosphere at the present time. Analysis and understanding of the radiative forcings owing to the direct and indirect aerosol climate effects require the basic scattering and absorption properties. The dust storms originating in China during the springtime and their global transport have a profound impact on the climate of East Asia. Moreover, China is the largest underdeveloped country in the world and has been obtaining 80% of its energy from coal combustion. The emission of BC has been especially large owing to low-temperature household coal burning. Dust and BC are nonspherical and inhomogeneous particles. Reliable and efficient determination of the scattering and absorption properties of these particles based on theoretical approach, numerical solution, and controlled laboratory experiment must be undertaken in order to reduce uncertainties in their radiative forcings by means of global and regional climate models.

The effect of terrain inhomogeneity on the radiation fields of the surface and the atmosphere above has not been accounted for in weather and climate models at this point. On the basis of a 3D radiative transfer program we illustrated that without consideration of topographical variability in typical midlatitute mountainous regions in the United States, net solar flux at the surface can be off by 5–20 $\mathrm{W/m^2}$, assuming a flat surface. Many landscapes on the continents exhibit significant terrain features and in particular, the Tibetan Plateau has a profound influence on the general circulation of the atmosphere and climate in the East Asia region. The temporal and spatial distributions of surface radiation over this intensive topography determine surface dynamic processes and atmospheric radiative heating. Thus, accurate calculations and parametrizations of radiative transfer including both the solar and the thermal infrared spectra in clear and cloudy conditions must be developed for incorporation in regional and global models.

The last unsolved radiative transfer area we identified is associated with the transfer of solar radiation in the atmosphere–ocean system. The ocean covers about 70% of the Earth's surface, and the radiation interface between the atmosphere and the ocean is rather intricate. We pointed out that the vertical distribution of solar flux influences the stability and stratification of the mixed layer and the sea surface temperature. The surface roughness produced by the winds is the predominating factor controlling the penetration of solar flux into the ocean mixed layer and it must be correctly modeled for radiation calculations. Finally, we pointed out the lack of fundamental scattering and absorption information on irregular phytoplankton and other species in the ocean for heating rate calculation and remote sensing application.

Acknowledgements

The research for this work has been supported in part by NSF Grants ATM-0331550 and ATM-0437349 and DOE Grant DE-FG03-00ER62904. We thank Yoshihide Takano and Rick Hansell for their assistance during the preparation of this article.

[Received 4 January 2007; Revised 28 April 2007; Accepted 30 April 2007.]

References

Chandrasekhar, S., 1950: *Radiative Transfer.* Oxford University Press, Oxford, 393 pp.

Charney, J., and A. Elliassen, 1949: A numerical method for predicting the perturbations of middle latitude westerlies. *Tellus*, **1**(2), 38–54.

Chen, Y., A. Hall, and K. N. Liou, 2006: Application of 3D solar radiative transfer to mountains. *J. Geophys. Res.*, **111**, D21111, doi:10.1029/2006JD007163.

Cox, C., and W. Munk, 1954: Measurement of the roughness of the sea surface from photographs of the sun's glitter. *J. Opt. Soc. Amer.*, **44**, 838–850.

d'Almeida, G. A., P. Koepke, and E. P. Shettle, 1991: *Atmospheric Aerosols: Global Climatology*

and Radiative Characteristics, A. Deepak Virginia, 561 pp.

Dozier, J., 1980: A clear-sky spectral solar radiation model for snow-covered mountainous terrain. *Water Resour. Res.*, **16**, 709–718.

Dozier, J., and J. Frew, 1990: Rapid calculations of terrain parameters for radiation modeling from digital elevation data. *IEEE Trans. Geosci. Remote Sens.,* **28**, 963–969.

Dubovik, O., A. Sinyuk, T. Lapyonok *et al.*, 2006: The application of spheroid models to account for aerosol particle nonsphericity in remote sensing of desert dust. *J. Geophys. Res.* **111**, D11208, doi:10.1029/2005JD006619.

Duguay, C., 1993: Radiation modeling in mountainous terrain: Review and status. *Mt Res. Dev.*, **13**, 339–357.

Falkovich, A. H., E. Ganor, Z. Levin, P. Formenti, and Y. Rudich, 2001: Chemical and mineralogical analysis of individual mineral dust particles. *J. Geophys. Res.*, **106**, 18029–18036.

Fu, Q., and K. N. Liou, 1992: On the correlated k-distribution method for radiative transfer in nonhomogeneous atmospheres. *J. Atmos. Sci.*, **49**, 2139–2156.

Fu, Q., and K. N. Liou, 1993: Parameterization of the radiative properties of cirrus clouds. *J. Atmos. Sci.*, **50**, 2008–2025.

Gao, Y., and J. R. Anderson, 2001: Characteristics of Chinese aerosols determined by individual particle analysis. *J. Geophys. Res.*, **106**, 18037–18045.

Giorgi, F., X. Bi, and Y. Qian, 2002: Direct radiative forcing and regional climatic effects of anthropogenic aerosols over East Asia: A regional coupled climate-chemistry/aerosol model study. *J. Geophys. Res.*, **107**, 4439, 10.1029/2001JD001066.

Gu, Y., J. Farrara, K. N. Liou, and C. R. Mechoso, 2003: Parameterization of cloud-radiation processes in the UCLA general circulation model. *J. Climate*, **16**, 3357–3370.

Gu, Y., K. N. Liou, Y. Xue, C. Mechoso, W. Li, and Y. Luo, 2006: Climatic effects of different aerosol types in China simulated by the UCLA atmospheric general circulation model. *J. Geophys. Res.,* **111**, D15201, doi:10.1029/2005JD006312.

IPCC, 2001: *Climate Change 2001: The Scientific Basis*, Houghton, J. T., Ding, Y., Griggs, D. J., Noguer, M., van den Linden, P. J., Dai, X., Johnson, C. A. (eds.), Intergovernmental Panel on Climate Change, Cambridge University Press, Cambridge, New York, 881 pp.

Jacobson, M. Z., 2001: Strong radiative heating owing to the mixing state of black carbon in the atmospheric aerosols. *Nature*, **409**, 695–697.

Jin, Z., T. P. Charlock, and K. Rutledge, 2002: Analysis of broadband solar radiation and albedo over the ocean surface at COVE. *J. Atmos. Oceanic Technol.*, **19**, 1585–1601.

Kalashnikova, O. V., and I. N. Sokolik, 2002: Importance of shapes and compositions of windblown dust particles for remote sensing at solar wavelengths. *Geophys. Res. Lett.*, **29**, 10.1029/2002GL014947.

Koren, I., E. Ganor, and J. H. Joseph, 2001: On the relation betweens size and shape of desert dust aerosol, *J. Geophys. Res.*, **106**, 18047–18054.

Koren, I., Y. J. Kaufman, L. A. Remer, and J. V. Martins, 2004: Measurements of the effect of Amazon smoke on inhibition of cloud formation. *Science*, **303**, 1342–1345.

Lee, W., and K. N. Liou, 2007: A coupled atmosphere–ocean radiative transfer system using the analytic four-stream approximation. *J. Atmos. Sci.*, **64**, 3681–3694.

Liou, K. N., 1974: Analytic two-stream and four-stream solutions for radiative transfer. *J. Atmos. Sci.*, **31**, 1473–1475.

Liou, K. N., 1980: *An Introduction to Atmospheric Radiation*. Academic, New York, 392 pp.

Liou, K. N., 2002: *An Introduction to Atmospheric Radiation*, 2nd edition. Academic, San Diego, 583 pp.

Liou, K. N., Q. Fu, and T. P. Ackerman, 1988: A simple formulation of the delta-four-stream approximation for radiative transfer parameterizations. *J. Atmos. Sci.*, **45**, 1940–1947.

Liu, L., and M. I. Mishchenko, 2005: Effects of aggregation on scattering and radiative properties of soot aerosols. *J. Geophys. Res.*, **110**, D11211.

Luo, Y., D. Lu, X. Zhou, W. Li, and Q. He, 2001: Characteristics of the spatial distribution and yearly variation of aerosol optical depth over China in last 30 years, *J. Geophys. Res.*, **106**, 14501–14513.

Marshak, A., and A. B. Davis (eds.), 2005: *3D Radiative Transfer in Cloudy Atmospheres.* Springer-Verlag, Berlin, 686 pp.

Martins, J. V., P. Artaxo, C. Liousse *et al.*, 1998: Effects of black carbon content, particle size, and mixing on light absorption by aerosols from

biomass burning in Brazil. *J. Geophys. Res.*, **103**, 32041–32050.

Menon, S., J. Hansen, L. Nazarenko, and Y. Luo, 2002: Climate effects of black carbon aerosols in China and India. *Science*, **297**, 2250–2253.

Mishchenko, M. I., A. A. Lacis, B. E. Carlson, and L. D. Travis, 1995: Nonsphericity of dust-like tropospheric aerosols: Implications for aerosol remote sensing and climate modeling. *Geophy. Res. Lett.*, **22**, 1077–1080.

Mishchenko, M. I., L. D. Travis, and D. W. Mackowski, 1996: T-matrix computation of light scattering by nonspherical particles: A review, *J. Quant. Spectrosc. Radiat. Transfer*, **55**, 535–575.

Miesch, C., X. Briottet, Y. H. Herr, and F. Cabot, 1999: Monte Carlo approach for solving the radiative transfer equation over mountainous and heterogeneous areas. *Appl. Opt.*, **38**, 7419–7430.

Mobley, C. D., 1994: *Light and Water: Radiative Transfer in Natural Waters*. Academic, San Diego, 592 pp.

Morel, A., and S. Maritorena, 2001: Bio-optical properties of oceanic waters: A reappraisal. *J. Geophys. Res.*, **106**, 7163–7180.

Ohlmann, J. C., D. A. Siegel, and C. Gautier, 1996: Ocean mixed layer radiant heating and solar penetration: A global analysis. *J. Climate*, **9**, 2265–2280.

Okada, K., J. Heintzenberg, K. Kai, and Y. Qin, 2001: Shape of atmospheric mineral particles collected in three Chinese arid regions. *Geophys. Res. Lett.*, **28**, 3123–3126.

Olyphant, G. A., 1986: The components of incoming radiation within a mid-latitude alpine watershed during the snowmelt season. *Arct. Alp. Res.*, **18**, 163–169.

Preisendorfer, R. W., and C. D. Mobley, 1985: Unpolarized irradiance reflectances and glitter patterns of random capillary waves on lakes and seas by Monte Carlo simulation. NOAA Tech. Memo, ERL PMEL-63, Pacific Mar. Environ. Lab., Seattle, WA, 141 pp.

Reid, J. S., P. V. Hobbs, C. Liousse *et al.*, 1998: Comparisons of techniques for measuring shortwave absorption and black carbon content of aerosols from biomass burning in Brazil. *J. Geophys. Res.*, **103**, 32031–32040.

Reid, J. S., H. H. Jonsson, H. B. Maring *et al.*, 2003: Comparison of size and morphological measurements of coarse mode dust particles from Africa. *J. Geophys. Res.*, **108**, doi:10.1029/2002JD002485.

Rosen, H., and T. Novakov, 1984: Role of graphitic carbon particles in atmospheric radiation on transfer. In *Aerosols and their Climatic Effects*. H. E. Gerber and A. Deepak (eds.), Virginia, pp. 83–94.

Scholes, M., and M. O. Andreae, 2000: Biogenic and pyrogenic emissions from Africa and their impact on the global atmosphere. *Ambio*, **29**, 23–29.

Siege, D. A., J. C. Ohlmann, L. Washburn *et al.*, 1995: Solar radiation, phytoplankton pigments, and radiant heating of the equatorial Pacific warm pool. *J. Geophys. Res.*, **100**, 4885–4891.

Smith, R. C., and K. S. Baker, 1981: Optical properties of the clearest natural waters (200–800 nm). *Appl. Opt.*, **20**, 177–184.

Sokolik, I. N., O. B. Toon, and R. W. Bergstrom 1998: Modeling the radiative characteristics of airborne mineral aerosols at infrared wavelengths. *J. Geophys. Res.*, **103**, 8813–8826.

Sokolik, I. N., D. M. Winker, G. Bergametti *et al.*, 2001: Introduction to spectral section: Outstanding problems in quantifying the radiative impact of mineral dust, *J. Geophys. Res.*, **106**, 18015–18027.

Streets, D. G., S. Gupta, S. T. Waldhoff *et al.*, 2001: Black carbon emissions in China. *Atmos. Environ.*, **35**, 4281–4296.

Wu, J., W. Jiang, C. Fu, B. Su, H. Liu, and J. Tang, 2004: Simulation of the radiative effect of black carbon aerosols and the regional climate response over China. *Adv. Atmos. Sci.*, **21**, 637–649.

Yang, P., and K. N. Liou, 2000: Finite difference time domain method for light scattering by nonspherical particles. In *Light Scattering by Nonspherical Particles: Theory, Measurements, and Geophysical Applications*, M. Mishchenko *et al.* (eds.), Academic, San Diego, pp. 173–221.

Ye, D. (Yeh, T. C.), 1979: *The Meteorology of Qinghai–Xizang Plateau*, D. Ye and Y. X. Gao (eds.) Chap. 1, Science Press, Beijing (in Chinese).